
Article:
Wang, Yuan, Song, Xiaoxiao, Xi, Jingqian et al. (2022) A Resonant Lorentz-Force Magnetometer Exploiting Blue Sideband Actuation to Enhance Sensitivity and Resolution. Journal of Microelectromechanical Systems. ISSN: 1941-0158

A Resonant Lorentz-Force Magnetometer Exploiting Blue Sideband Actuation to Enhance Sensitivity and Resolution

Yuan Wang, Xiaoxiao Song, Jingqian Xi, Fangzheng Li, Lei Xu, Huafeng Liu, *Member*, Chen Wang, Shuangyang Kuang, Liangcheng Tu, Michael Kraft and Chun Zhao, *Senior Member*

***Abstract*—This paper reports a miniaturized resonant Lorentz-force magnetometer that exploits blue-sideband actuation to attain a better sensitivity and resolution. The resonant magnetometer consists of a double-ended tuning fork (DETF) resonator with cavity slots to optimize thermoelastic dissipation, as well as a Lorentz-force generator structure to transduce the magnetic force to the axial of the resonator. The proposed device demonstrates a Lorentz-force sensitivity of 5.5 mV/nN, a noise floor of 1.25 μV/ √ Hz, and a resolution of 0.23 pN/ √ Hz. In comparison with a conventional drive scheme, the blue-sideband actuation achieves approximately two orders of magnitude improvement regarding sensitivity and resolution than that of the amplitude modulation (AM) readout and 3.6-fold enhancement than that of the frequency modulation (FM) readout. The results affirm the merit of the novel excitation method and provide solid evidence of its effectiveness in practical applications.**

***Index Terms*—Blue-sideband actuation; Magnetometer; Double-ended tuning fork; Lorentz-force**

I. Introduction

Micro-electro-mechanical-system (MEMS) resonators are widely employed as physical sensors benefiting from fabrication compatibility and good performance metrics. Resonant magnetometers are a type of resonant sensor that have attracted extensive scientific interest. A MEMS resonant Lorentz-force magnetometer responds to variations of the external magnetic field, implementing transduction from a physical force to an electrical readout. In comparison with other types of magnetometers, for instance, magnetoresistive and Hall-effect sensors, MEMS resonant Lorentz-force magnetometers are advantageous in dynamic range and free of magnetic hysteresis [1]. In accordance with the readout scheme, resonant Lorentz-force magnetometers can be classified as AM and FM devices. Both approaches have unique merits and the debate about superiority remains unresolved. AM devices usually are regarded to have higher sensitivity [2]–[8] while FM devices have a larger dynamic range and better stability [9]–[12]. Furthermore, novel actuation methods [13]–[18] for micro-resonator have been explored, to supersede the common AC excitation of which the drive frequency is near the resonant frequency of the resonator. Among them, blue-sideband actuation utilizes the summation of two vibration mode frequencies as drive frequency, facilitating suppression of the feedthrough signal. Nevertheless, this method remains in form of a concept study and is yet to be applied in a practical resonant sensor [19].

In this work, the blue-sideband actuation is adopted in a MEMS resonant Lorentz-force magnetometer. The experimental results confirm an improved performance compared to a conventional AC drive, using either AM or FM readout. The blue-sideband actuated resonant magnetometer yields a Lorentz-force sensitivity of 5.5 mV/nN, a noise floor of 1.25 μV/√Hz, and a resolution of 0.23 pN/√Hz.

II. Device Description

The sensing element of the proposed resonant magnetometer is a micromachined DETF resonator, whose resonant frequency and vibration amplitude are modulated by the Lorentz force subjected to the external magnetic field. The schematic of the resonant Lorentz-force magnetometer is depicted in Fig. 1(a), in which a slotted DETF resonator is located between a set of transverse long beams. The transverse beams act as the Lorentz-force generator, providing a path of the injected current flow and hence deforming due to the induced magnetic Lorentz force. The resultant axial force acts on the tail of the DETF, modulating the effective stiffness of the resonator, and ultimately the resonant frequency and vibration amplitude of the DETF. Four electrodes are situated adjacent to the tine beams of the DETF, serving as motional current pick-up electrodes (Sense 1 and Sense 2 in Fig. 1) or drive electrodes. In this work, only one sense electrode was employed, whereas

This work was supported by the National Key Research and Development Program of China, Grant No. 2018YFB2002300. *(Corresponding authors: Huafeng Liu; Chen Wang; Shuangyang Kuang.)*

Y. Wang, X. Song, F. Li, L. Gao, L. Xu, J. Xi, H. Liu, S. Kuang, L. Tu and C. Zhao are with Huazhong University of Science and Technology, PGMF and School of Physics, MOE Key Laboratory of Fundamental Physical Quantities Measurement & Hubei Key Laboratory of Gravitation and Quantum Physics, Wuhan, China.

L. Tu is also affiliated with TianQin Research Center for Gravitational Physics and School of Physics and Astronomy, Sun Yat-sen University (Zhuhai Campus), Zhuhai, China.

C. Wang and M. Kraft are with University of Leuven, Department of Electrical Engineering-MNS, Leuven, Belgium.

C. Zhao is also with Department of Electronics Engineering, University of York, Heslington, York, UK.

both drive electrodes were used for either AC or blue-sideband drive scheme. To be more specific, electrode Vac is used for the conventional AC drive scheme, where electrode Vblue remains disconnected; electrode Vblue is used for the blue-sideband excitation, in which electrode Vac is disconnected. The out-of-phase mode of the DETF is selected as working mode and the operation mechanism of the resonant magnetometer is illustrated in Fig. 1(b).

The cavity slots in the tine beams of the DETF can optimize the thermal elastic dissipation of the resonator effectively, resulting in an enhancement of the quality factor (Q-factor). This approach helps to solve the compromise required between the device Q-factor and structure complexity, as well as the need of sealed vacuum encapsulation. Without altering the geometry of the device, an improvement of the Q-factor of about 5.9-fold was achieved in previous work [20], compared to a common DETF resonant magnetometer with the same parameters.

The proposed device was fabricated by a commercial SOI process available from MEMSCAP [20]. The dimensional parameters of the resonant magnetometer are listed in Table I, and the scanning electron microscope (SEM) graphs of the fabricated device are shown in Fig. 1(c).

TABLE I
Device dimensions

Name	Parameter	Value
Lorentz-force generator	Beam length	2000 μm
	Beam width	10 μm
DETF	Tine length	740 μm
	Tine width	15 μm
	Slot length	320 μm
	Slot width	3 μm
Device thickness	Thickness	25 μm
Capacitive air gap	Width	2 μm

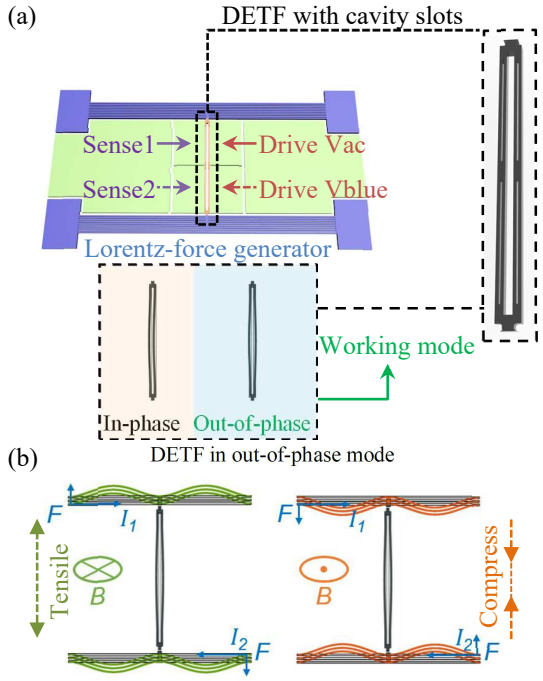

(c)

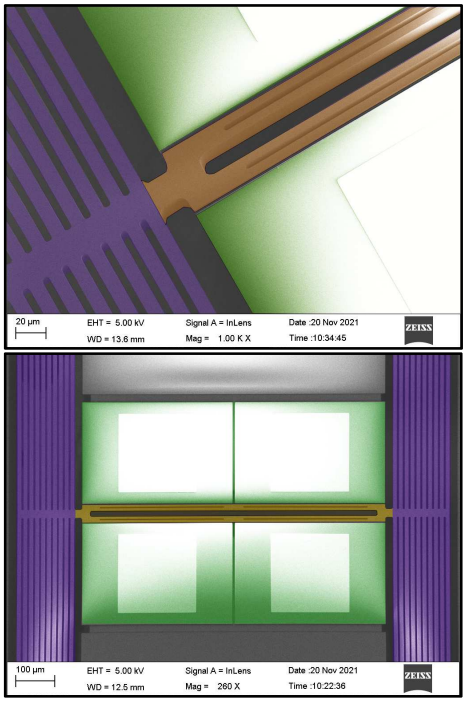

Fig. 1. Basics of the device: (a) schematic of the resonant Lorentz-force magnetometer; (b) working mechanism of the device, where *F* and *I* are the Lorentz-force and current flow, respectively; (c) SEM graphs of the fabricated device.

III. Experimental Setup

In both drive schemes, a polarization voltage V_{DC} was applied to the device, which also provided the current flow through the Lorentz-force generator. The potential difference across the Lorentz-force generator was 8 V, the measured resistance between the two ports of the generator was ~110 Ω, and a 1 kΩ resistor was added to limit the current magnitude. The initial current flow therefrom was 7.2 mA, which agreed well with actual measurements. The conventional AC actuation was set up by a V_{AC} component with a magnitude of 8 mV generated from a lock-in amplifier (MFLI, Zurich Instruments). For the blue-sideband actuation, a function generator was employed, of which the excitation amplitude was a tunable parameter whereas the drive frequency was maintained as the sum of the in- and out-of-phase mode frequencies of the DETF. A vacuum chamber with a pressure level of 1 Pa was used and room temperature was maintained for all following experiments. The data acquisition was done by the MFLI instrument, and post-processing in Matlab. The interface circuitry of the magnetometer was assembled on a PCB, comprising the carrier of the MEMS device and the electronic components. The output motional current of the resonant magnetometer was converted and amplified by a transimpedance amplifier, with a gain of 5×10^6 Ω. The PCB and the permanent magnet were assembled on a 3D-printed holder, which was placed in the vacuum chamber during the experiments, as illustrated in Fig. 2(a). Performance characterizations were carried out using a MFLI lock-in amplifier; the experimental setup is shown in Fig. 2(b). Closed-loop operation was realized by using the PID/PLL

module of the MFLI lock-in amplifier, with a bandwidth of 10 Hz and a sampling frequency of 200 Hz.

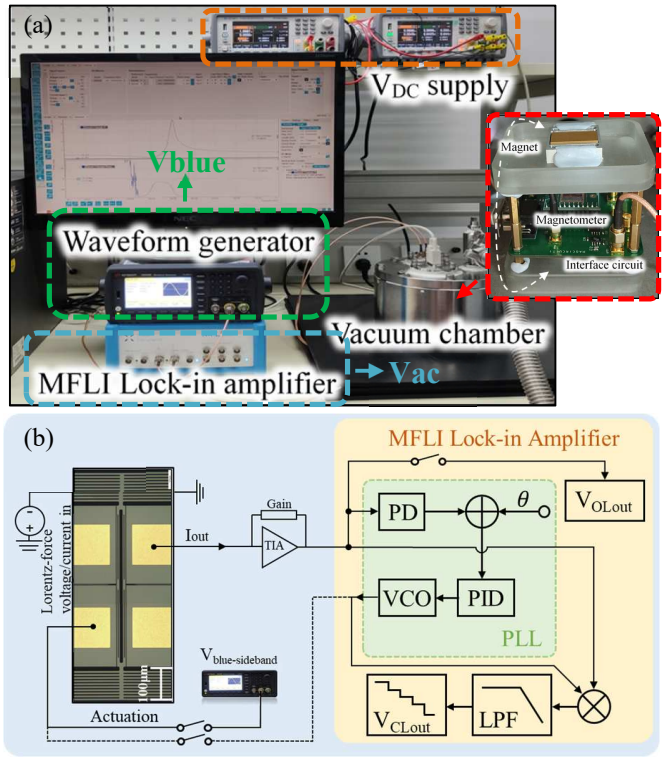

Fig. 2. Measurement set-up: (a) experimental platform. (b) schematic of the experimental set-up.

IV. Experimental Results

A. Performance characterization

The proposed resonant Lorentz-force magnetometer was first tested by using a conventional AC drive scheme with an amplitude of V_{ac}=8 mV. A frequency-amplitude response was obtained by a frequency sweep using the MFLI lock-in amplifier, in an open-loop configuration, as shown in Fig. 3 (a), of which the in-phase mode yielded a resonant frequency of 102.059 kHz, a Q-factor of 26600 and the out-of-phase mode yielded a resonant frequency of 104.433 kHz, a Q-factor of 38100, operating under a vacuum condition of 1 Pa. The blue-sideband actuation scheme was conducted with a frequency equal to the sum of the in-phase and the out-of-phase modes frequencies of the DETF, $f_{blue}=f_{inphase}+f_{outofphase}$=206.492 kHz, and an amplitude V_{blue}=150 mV, under a fixed magnetic field of 38 mT. Measurements for consecutive Lorentz forces were carried out subsequently, in which the varying Lorentz force was induced by tuning the potential difference across the Lorentz-force generator, resulting in a current change from 7.2 mA to 7.29 mA, with a 0.009 mA step; this is equivalent to a Lorentz force change from 0.547 μN to 0.554 μN, with a 0.684 nN step. The results are shown in Fig. 3(b) and Fig. 3(c). The experimental data regarding blue-sideband actuation was obtained by amplitude modulation in the MFLI lock-in amplifier in an open-loop configuration. It is also worth mentioning that the blue-sideband actuation scheme simultaneously excited both the in-phase and the out-of-phase modes of the resonator, while during the experiment, we focused on the out-of-phase mode region.

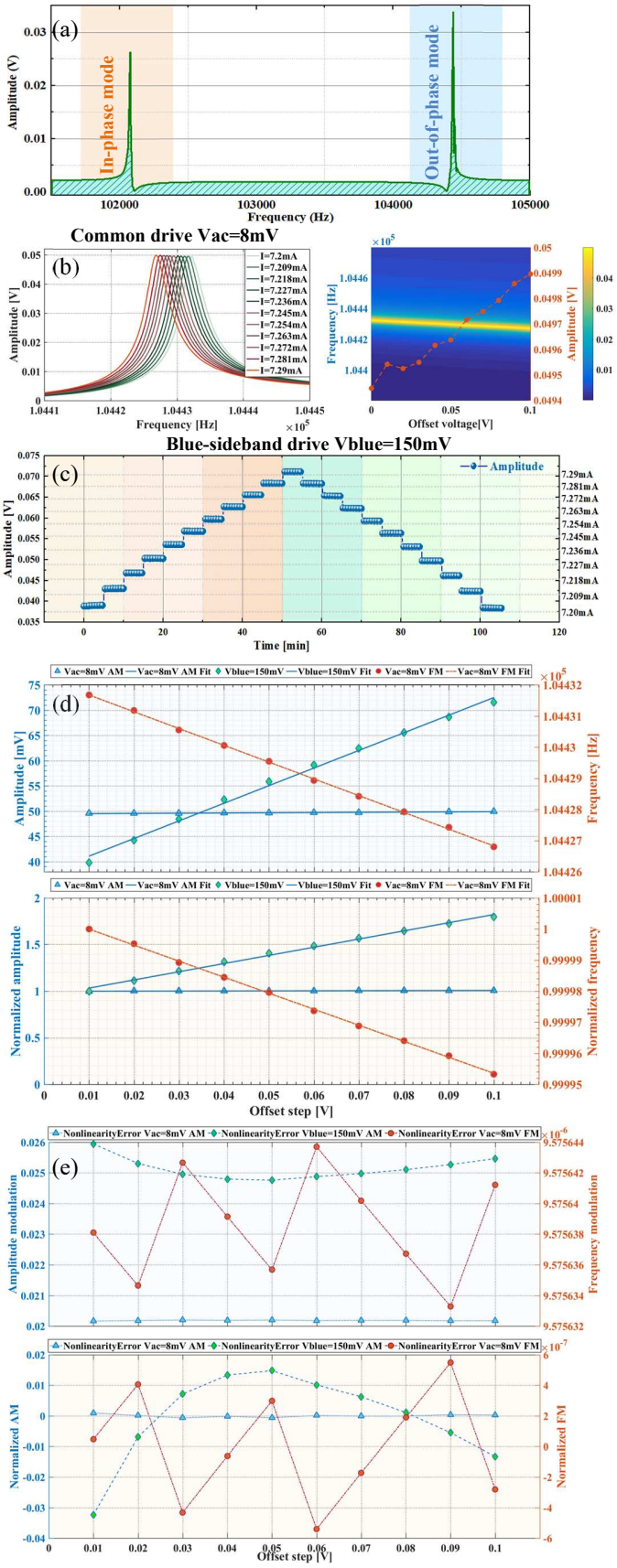

Fig. 3. Sensitivity characterizations: (a) frequency sweep of the tested device. (b) frequency responses of the AC drive scheme subjected to a consecutive Lorentz-force perturbation. (c) amplitude responses of the blue-sideband drive scheme subjected to a consecutive Lorentz-force. (d) sensitivity and normalized sensitivity comparisons. (e) linearity errors.

A sensitivity comparison was then carried out, including a conventional AC actuation with both AM and FM readout metrics, and the blue-sideband actuation using AM readout; this is shown in Fig. 3(d), whereas the linearity errors are plotted in Fig. 3(e). The computed relative and absolute sensitivities are summarized in Table II.

TABLE II
Comparisons of sensitivity

	Relative sensitivity	Absolute sensitivity
V_{ac}-AM	900 ppm	0.0651 mV/nN
V_{ac}-FM	5 ppm	0.78 Hz/nN
V_{blue}-AM	0.11 (110000 ppm)	5.5 mV/nN

The noise performance of the proposed resonant magnetometer using blue-sideband actuation was captured. The recorded data are shown in Fig. 4 (a), and the Allan deviation (AD) are illustrated in Fig. 4 (b). The obtained noise floor, stability and resolution are summarized in Table III. The minimum noise floor level was determined in the band between 1 Hz and 10 Hz from the PSD, and the stability was evaluated in the region of 0.1 s to 1 s in the AD, for both AM and FM schemes. The comparison was based on the selected frequency around 3.1 Hz in the PSD, corresponding to the stability around 0.32 s in the AD.

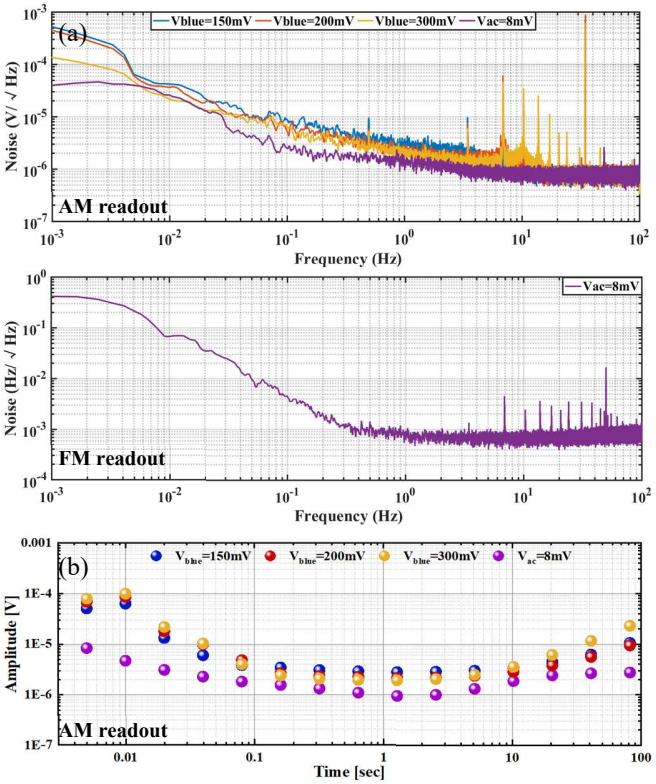

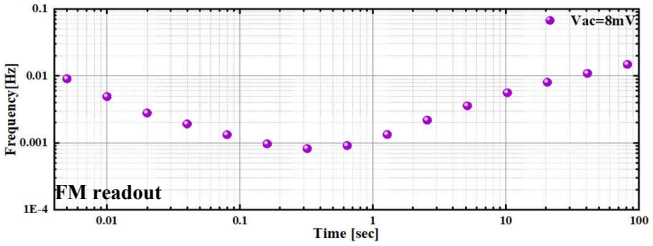

Fig. 4. Noise characterizations: (a) noise PSD with respect to AM and FM readout, including blue-sideband drive and AC drive. (b) AD with respect to AM and FM readout, including blue-sideband drive and AC drive, where the FM readout was captured using a closed-loop configuration.

TABLE III
Noise and resolution comparison

	Noise floor	Stability	Resolution
V_{ac}-AM	0.94 μV/ √ Hz	1.33 μV	14.44 pN/ √ Hz
V_{ac}-FM	650 μHz/ √ Hz	820 μHz	0.83 pN/ √ Hz
V_{blue}-AM	1.25 μV/ √ Hz	2.07 μV	0.23 pN/ √ Hz

B. Dynamic characterization

The dynamic responses of the proposed resonant magnetometer were recorded by introducing a periodic Lorentz force perturbation. An offset voltage across the Lorentz-force generator with an amplitude of 10 mV was selected, whereas its frequency was a tunable parameter. In the following experiments, the periodic Lorentz force was configured with frequencies of 0.1 Hz, 0.5 Hz, 1 Hz, 5 Hz and 10 Hz, respectively. The amplitude of the device by using the blue-sideband actuation subsequently responded to the input Lorentz force and changed with the same frequency pattern. The captured data are shown in Fig. 5 (a), and the PSD after introducing the periodic Lorentz force is illustrated in Fig. 5 (b).

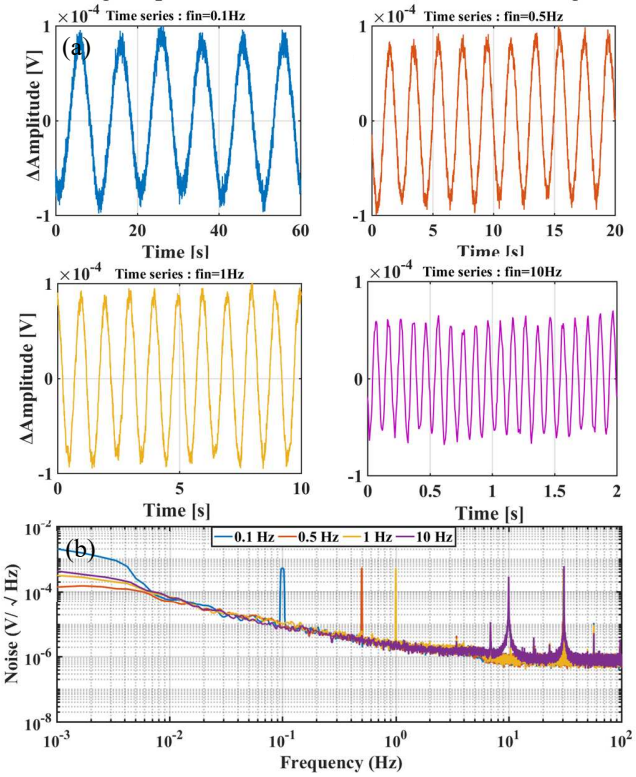

Fig. 5. Dynamic characterizations: (a) measured time series with respect to different frequencies of the Lorentz force. (b) noise PSD with respect to different frequencies of the Lorentz force.

In this experiment, the functionality of handling dynamic input of the proposed device featuring blue-sideband actuation is validated. Both the time series and PSD below 1 Hz confirm the performance of the subject, albeit attenuation of the amplitude is observed above 1 Hz. This could be attributed to the bandwidth of the measurement facility, further exploration is required to investigate this phenomenon.

V. Conclusion

In this work, a MEMS resonant Lorentz-force magnetometer is excited by exploiting a blue-sideband scheme. As a result, the performance of the resonant magnetometer is boosted significantly. In particular, the acquired absolute sensitivity in terms of AM readout is 5.5 mV/nN, which is approximately two orders of magnitudes higher than that of the conventional AC drive scheme using AM readout. The relative sensitivity, on the other hand, is 0.11, that is, 119 times higher than that of a conventional AC drive scheme using AM readout, and 21348 times higher than that of the FM readout. The comparison of resolution also proves the superiority of the blue-sideband actuation, in which the drive using AM readout attains a resolution of 0.23 pN/ √ Hz, which is a 63-fold improvement in contrast with the common AC drive scheme using AM readout, and a 3.6-fold improvement compared to the FM readout. Another important property of this technique is the universality as the blue-sideband actuation can be employed in other types of micro-resonators, covering a broad range of applications, for example, atomic force microscopy (AFM), resonant accelerometers and gyroscopes. The observed disadvantage of the blue-sideband actuation is the nonlinearity, which is worse compared to the convention AC scheme. Future work should focus on designing and optimizing the electronics dedicated for the blue-sideband actuation, which is expected to reduce significantly the noise floor. Further exploration of the dynamic behaviour for this subject is another task, as well as developing the integrated module of the blue-sideband actuation.

References

[1] M. Li, V. Rouf, M. Thompson, and D. Horsley, "Three-axis Lorentz-force magnetic sensor for electronic compass applications," *Journal of Microelectromechanical Systems*, vol. 21, no. 4, pp. 1002-1010, 2012.

[2] C. R. Marra, G. Laghi, M. Gadola, G. Gattere, D. Paci, A. Tocchio, and G. Langfelder, "100 nT/√Hz, 0.5 mm 2 monolithic, multi-loop low-power 3-axis MEMS magnetometer," in *2018 IEEE Micro Electro Mechanical Systems (MEMS)*, 2018: IEEE, pp. 101-104.

[3] C. R. Marra, M. Gadola, G. Laghi, G. Gattere, and G. Langfelder, "Monolithic 3-axis MEMS multi-loop magnetometer: A performance analysis," *Journal of Microelectromechanical Systems*, vol. 27, no. 4, pp. 748-758, 2018.

[4] P. Minotti, S. Brenna, G. Laghi, A. G. Bonfanti, G. Langfelder, and A. L. Lacaita, "A Sub-400-nT/√Hz, 775-μW, Multi-Loop MEMS Magnetometer With Integrated Readout Electronics," *Journal of Microelectromechanical Systems*, vol. 24, no. 6, pp. 1938-1950, 2015.

[5] G. Laghi, C. R. Marra, P. Minotti, A. Tocchio, and G. Langfelder, "A 3-D micromechanical multi-loop magnetometer driven off-resonance by an on-chip resonator," *Journal of Microelectromechanical Systems*, vol. 25, no. 4, pp. 637-651, 2016.

[6] A. Herrera-May, P. Garcia-Ramirez, L. Aguilera-Cortes, J. Martinez-Castillo, A. Sauceda-Carvajal, L. Garcia-Gonzalez, and E. Figueras-Costa, "A resonant magnetic field microsensor with high quality factor at atmospheric pressure," *Journal of Micromechanics and Microengineering*, vol. 19, no. 1, p. 015016, 2008.

[7] M. Thompson and D. Horsley, "Parametrically amplified z-axis Lorentz force magnetometer," *Journal of microelectromechanical systems*, vol. 20, no. 3, pp. 702-710, 2011.

[8] S. Sonmezoglu, I. B. Flader, Y. Chen, D. D. Shin, T. W. Kenny, and D. A. Horsley, "Dual-resonator MEMS magnetic sensor with differential amplitude modulation," in *2017 19th International Conference on Solid-State Sensors, Actuators and Microsystems (TRANSDUCERS)*, 2017: IEEE, pp. 814-817.

[9] B. Bahreyni and C. Shafai, "A resonant micromachined magnetic field sensor," *IEEE Sensors Journal*, vol. 7, no. 9, pp. 1326-1334, 2007.

[10] N. Alcheikh and M. I. Younis, "Resonator-Based Bidirectional Lorentz Force Magnetic Sensor," *IEEE Electron Device Letters,* vol. 42, no. 3, pp. 406-409, 2021.

[11] N. Alcheikh, S. B. Mbarek, H. Ouakad, and M. I. Younis, "A highly sensitive and wide-range resonant magnetic micro-sensor based on a buckled micro-beam," *Sensors and Actuators A: Physical,* vol. 328, p. 112768, 2021.

[12] S. Sonmezoglu, I. B. Flader, Y. Chen, D. D. Shin, T. W. Kenny, and D. A. Horsley, "Dual-resonator MEMS Lorentz force magnetometer based on differential frequency modulation," in *2017 IEEE International Symposium on Inertial Sensors and Systems (INERTIAL)*, 2017: IEEE, pp. 160-163.

[13] J. M. L. Miller, A. Ansari, D. B. Heinz, Y. Chen, I. B. Flader, D. D. Shin, L. G. Villanueva, and T. W. Kenny, "Effective quality factor tuning mechanisms in micromechanical resonators," *Applied Physics Reviews*, vol. 5, no. 4, p. 041307, 2018.

[14] T. Miao, X. Hu, X. Zhou, X. Wu, Z. Hou, and D. Xiao, "A million-order effective quality factor MEMS resonator by mechanical pumping," in *2020 IEEE International Symposium on Inertial Sensors and Systems (INERTIAL)*, 2020: IEEE, pp. 1-4.

[15] N. Jaber, A. Ramini, Q. Hennawi, and M. I. Younis, "Wideband MEMS resonator using multifrequency excitation," *Sensors and Actuators A: Physical,* vol. 242, pp. 140-145, 2016.

[16] W. J. Venstra, H. J. Westra, and H. S. van der Zant, "Q-factor control of a microcantilever by mechanical sideband excitation," *Applied Physics Letters,* vol. 99, no. 15, p. 151904, 2011.

[17] X. Dong, M. I. Dykman, and H. B. Chan, "Strong negative nonlinear friction from induced two-phonon processes in

vibrational systems," *Nature communications,* vol. 9, no. 1, pp. 1-8, 2018.

[18] C. Li, J. Xi, Y. Wang, F. Li, L. Gao, H. Liu, C. Zhao, and L.-C. Tu, "On Enhancing the Sensitivity of Resonant Thermometers Based on Parametric Modulation," *Journal of Microelectromechanical Systems,* vol. 30, no. 4, pp. 539-549, 2021.

[19] A. Olkhovets, D. Carr, J. Parpia, and H. G. Craighead, "Non-degenerate nanomechanical parametric amplifier," in *Technical Digest. MEMS 2001. 14th IEEE International Conference on Micro Electro Mechanical Systems*, 2001: IEEE, pp. 298-300.

[20] Y. Wang, X. Song, F. Li, L. Gao, C. Li, J. Xi, H. Liu, C. Zhao, C. Wang, and L.-C. Tu, "A Resonant Lorentz-Force Magnetometer Featuring Slotted Double-Ended Tuning Fork Capable of Operating in a Bias Magnetic Field," *Journal of Microelectromechanical Systems,* vol. 30, no. 6, pp. 958-967, 2021.